Electronic Supplementary Information for

QM/MM and MM MD simulations on decontamination of the V-type nerve agent VX by phosphotriesterase: Toward a comprehensive understanding of steroselectivity and activity

Fangfang Fan,[a,b] Yongchao Zheng,*[,c] Yuzhuang Fu,[b] Yuwei Zhang,[b] He Zheng,[c] Changjiang Lyu,[a] Linyu Chen, [a] Jun Huang,*[,a] Zexing Cao*[,b]

[a]Key Laboratory of Chemical and Biological Processing Technology for Farm Products of Zhejiang Province, Zhejiang Provincial Collaborative Innovation Center of Agricultural Biological Resources Biochemical Manufacturing, School of Biological and Chemical Engineering, Zhejiang University of Science and Technology, Hangzhou 310023, People's Republic of China

[b]State Key Laboratory of Physical Chemistry of Solid Surfaces and Fujian Provincial Key Laboratory of Theoretical and Computational Chemistry, College of Chemistry and Chemical Engineering, Xiamen University, Xiamen 360015, People's Republic of China.

[c]State Key Laboratory of NBC Protection for Civilian, Beijing 102205, People's Republic of China.

*E-mail: zxcao@xmu.edu.cn (Z.C)

Table of contents

1. Substrate transportation and binding to the active site

The representative configurations of the substrate delivery to the active site for both R_P-VX and S_P-VX have been shown in Figure S1. For the R_P-VX, the substrate is completely free in the water solvent outside the pocket when $RC1_{Rp} \geq 8.5$ Å, and then the R_P-VX substrate gradually approaches the active pocket as the coordinate distance decreases. When the substrate molecule is close to the pocket (8.5 Å > $RC1_{Rp} \geq 5.8$ Å), it may adjust its orientation to fit with the active-site environment, where the bulky tail faces the leaving pocket, and the large and small substituents approach toward the large and small pockets respectively, forming an initial configuration favorable for the substrate entry into the active pocket ($RC1_{Rp}$ = 7.7 Å). Under the electrostatic interaction of the metal zinc ions, the carbonyl oxygen and Zn_β form an interaction mediated by a water molecule to guide the substrate into the pocket ($RC1_{Rp}$ = 6.5 Å). At $RC1_{Rp}$ = 6.3 Å, there is the strong electrostatic interaction directly between the substrate and Zn_β. Once the substrate completely enters the active pocket, the substrate posture is further adjusted for the binding interaction with the active site (5.8 Å > $RC1_{Rp}$ ≥ 4.5 Å). At $RC1_{Rp}$ = 4.5 Å, the substrate reaches an optimal binding site, where the large substituent is just in the large pocket, the small substituent is embedded in the small pocket buried deep inside the pocket, and the bulky leaving group falls into the leaving pocket.

For the S_P-VX with the same active site with the R_p-VX, denoted as the S_p-Model A, when $RC1_{Sp\text{-Model A}} \geq 9.2$ Å, the substrate is free in the solvent and gradually approaches the active pocket, while still maintaining the preferential orientation for the

substrate entry into the active pocket, like the R_P-VX transportation, where its large and small substituents are located towards the large and small pockets, respectively. When the S_P-enantiomer substrate further moves into the pocket (9.2 Å > $RC1_{Sp\text{-}Model\ A}$ ≥ 6.0 Å), the bulky leaving group still faces the leaving pocket, while the large and small substituents of the S_P-VX need to be flipped to adapt to the interaction between the substrate with the zinc ion through one water molecule, resulting in the small substituent in the large pocket, and the large substituent in the small pocket. Such entire turnover process needs to overcome free energy barriers of 1.5 ~ 3.1 kcal/mol respectively. At $RC1_{Sp\text{-}Model\ A}$ = 4.5 Å, the S_p-VX is completely bound to the active site with an energy release of 15.2 kcal/mol.

2. Estimation of the Binding Free Energy and its Decomposition Analysis

Here the trajectories from the last 20 ns MD simulations were used for the energy decomposition analysis and the estimation of the binding free energy for the enzyme-substrate interactions by Molecular Mechanics/Generalized Born Surface Area (MM/GBSA). This MM/GBSA method has been successfully applied to evaluate the relative binding free energy profiles for various ligand-protein complexes. The binding free energy is estimated by using a thermodynamic cycle that combines the energies from molecular mechanics with continuum solvent approaches, according to the equation:

$$\Delta G_{binding} = \Delta G_{complex} - \Delta G_{protein} - \Delta G_{ligand}$$

where $\Delta G_{complex}$, $\Delta G_{protein}$, and ΔG_{ligand} stand for the free energies of complex, receptor, and ligand, respectively. The free energy of each term can be estimated as the sum of three terms:

$$\Delta G_{binding} = \Delta E_{MM} + \Delta G_{sol} - T\Delta S$$

where ΔE_{MM} is the total gas phase energy expressed as the sum of the internal (int), electrostatic (ele), and van der Waals (vdW) energies:

$$\Delta E_{MM} = \Delta E_{int} + \Delta E_{ele} + \Delta E_{vdw}$$

$$\Delta G_{sol} = \Delta G_{GB} + \Delta G_{SA}$$

where ΔG_{sol} accounts for the polar (ΔG_{GB}) and non-polar (ΔG_{SA}) solvation energies. ΔG_{GB} is the polar contribution to the solvation free energy, described by the generalized Born (GB) calculation, while ΔG_{SA}, the non-polar solvation energy, is calculated from the solvent accessible surface area (SASA). $T\Delta S$ is the conformational entropy of binding and usually calculated by the normal-mode analysis.

In order to clarify the binding features of both R_p- and S_p-enantiomers of VX at the active site, the energy decomposition analyses have been performed, and the results are listed in Figure S2. Key constituents of the R_P-VX substrate nicely match the active pocket structurally, where the leaving pocket, the large pocket, and the small pocket accommodate corresponding groups of the substrate, respectively. The estimated binding free energy of -49.9 kcal/mol for the R_p-VX substrate, indicating stronger binding interactions with the active site than that for the S_P-enantiomer by 9.8 kcal/mol,

mainly contributed by its relatively stronger van der Waals and non-polar solvation interactions, as well as weaker polar solvation interactions, as shown in Figure S2. And interestingly, key residues to dominate the substrate binding are almost the same for both R_p-VX and S_p-VX, including His55, His57, His201, His230, Trp131, Lys169, and Asp301, where Lys169 is the most important.

3. Release of the Leaving Group

The release of leaving groups for the substrates Rp-VX and Sp-VX-Model B has been shown in Figure S9. For the R_P-model, at RC = 6.6 Å, five water molecules form a cluster surrounding the sulfur atom of the leaving group $DIAS^-$, where two water molecules are coordinated to Zn_β. At this time, the diameter of the pocket defined by the distance between F132 and L271 is about 15.0 ± 0.6 Å. At RC = 9.0 Å, more water molecules enter the pocket, and a relatively stable cluster of six water molecules to hydrate the leaving group is formed. At the same time, the newly added water molecules also replace the Zn_β-bound water molecules and maintain a six-coordinated Zn_β, avoiding structural fluctuation arising from the release of the leaving group, as shown by the diameter of the pocket of about 15.6 ± 0.6 Å. At RC = 13.0 Å, the diameter of the entrance pocket reaches the maximum value of 17.1 ± 0.9 Å, indicating that the leaving group passes across the narrowest part of the pocket. After the leaving group leaves away from the active pocket completely, the volume of the pocket shrinks, and the diameter of the pocket decreases to 11.7 ± 0.9 Å at RC = 14.0 Å. For the S_P-Model B, the pocket undergoes similar conformational change with the departure of the leaving group, where the pocket diameter gradually increases from 12.5 to 13.9 Å first,

and then decreases to about 11.0 Å after the release of the leaving group.

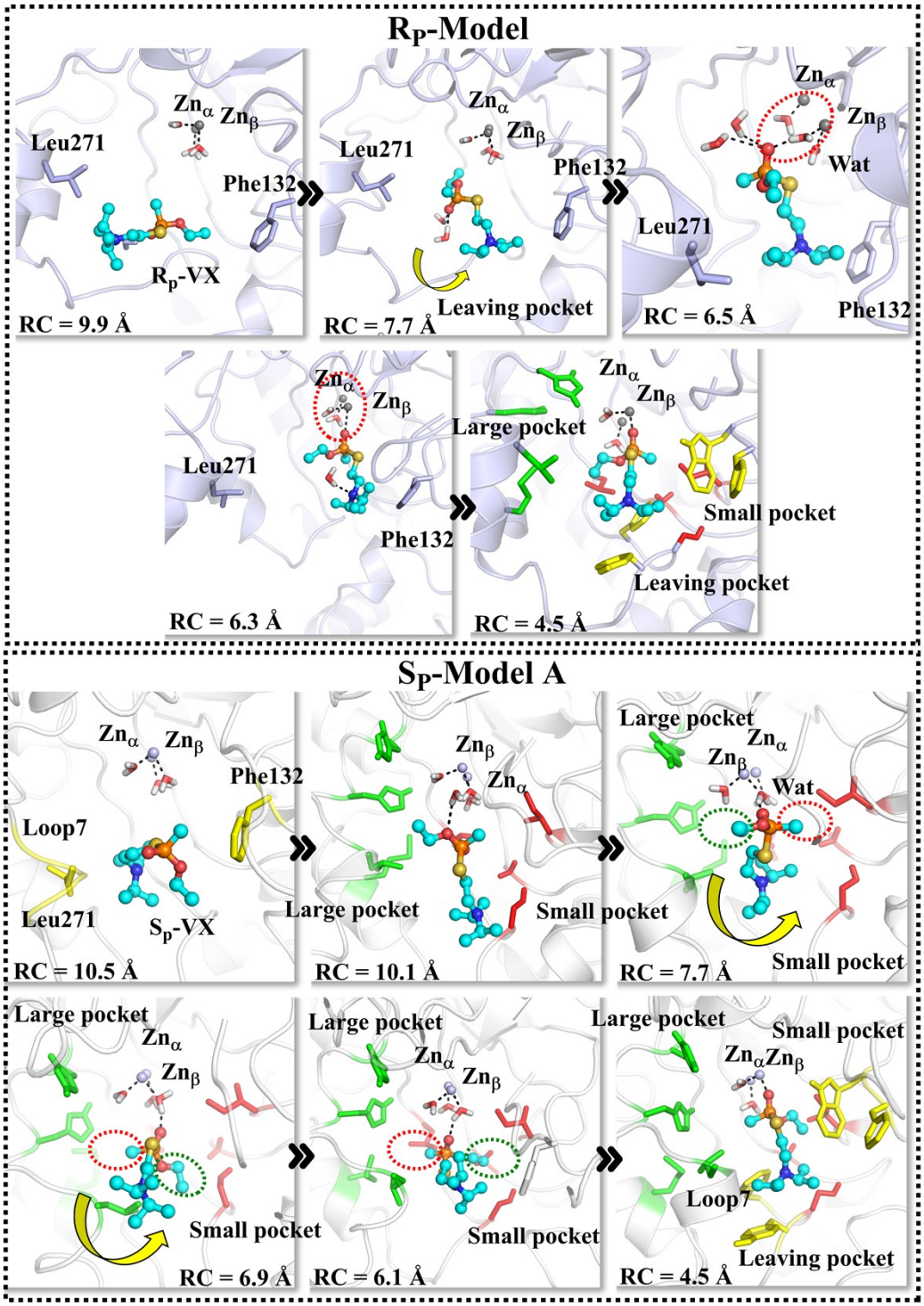

Figure S1. Representative structures and conformational changes of PTE-R_p-Model and S_p-VX-Model A systems during the substrate transportation to the active site.

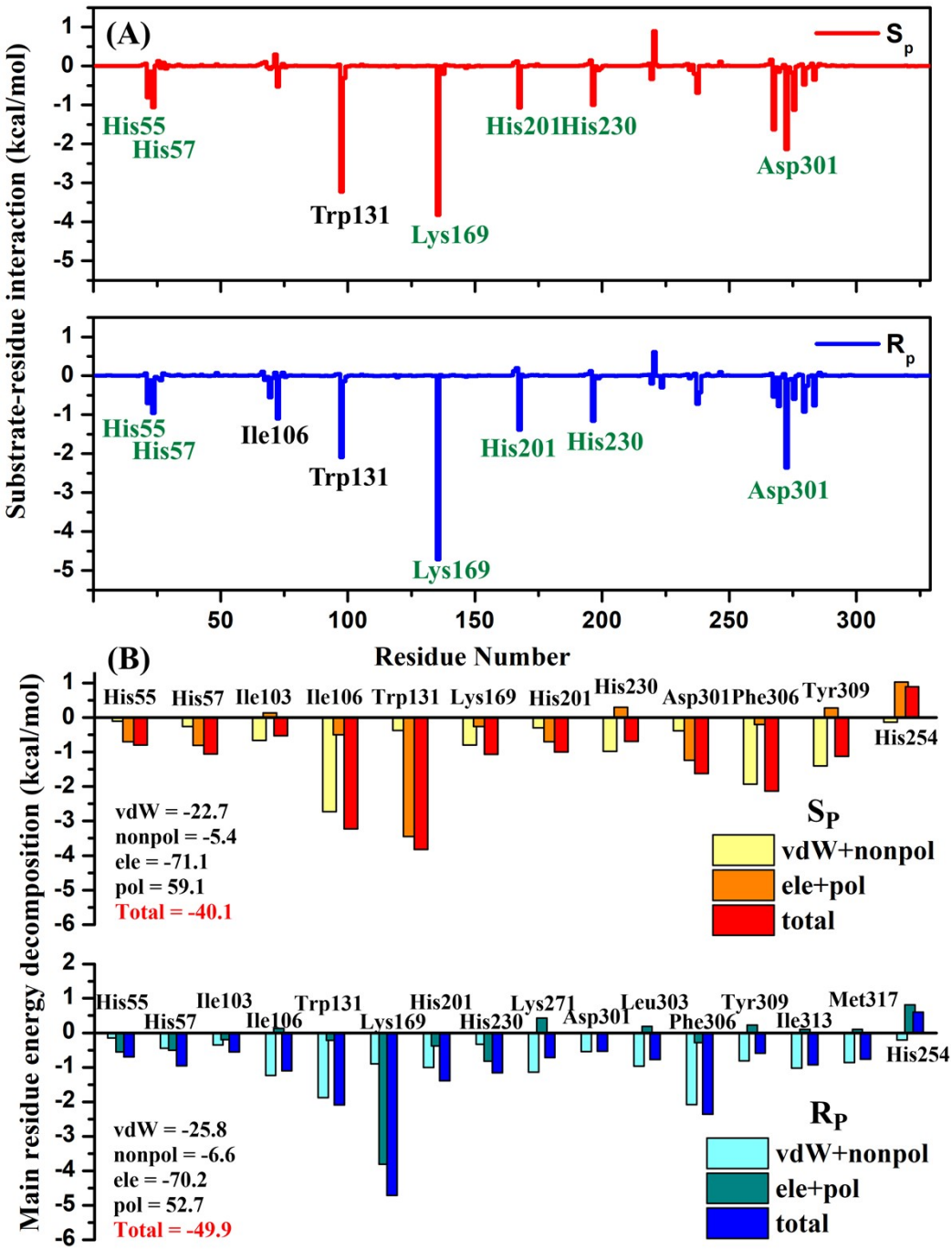

Figure S2. (A) The free energy decomposition on the basis of per-residue type for both enantiomers. (B) The energy decomposition for the key residues along with the free energy components for both enantiomers.

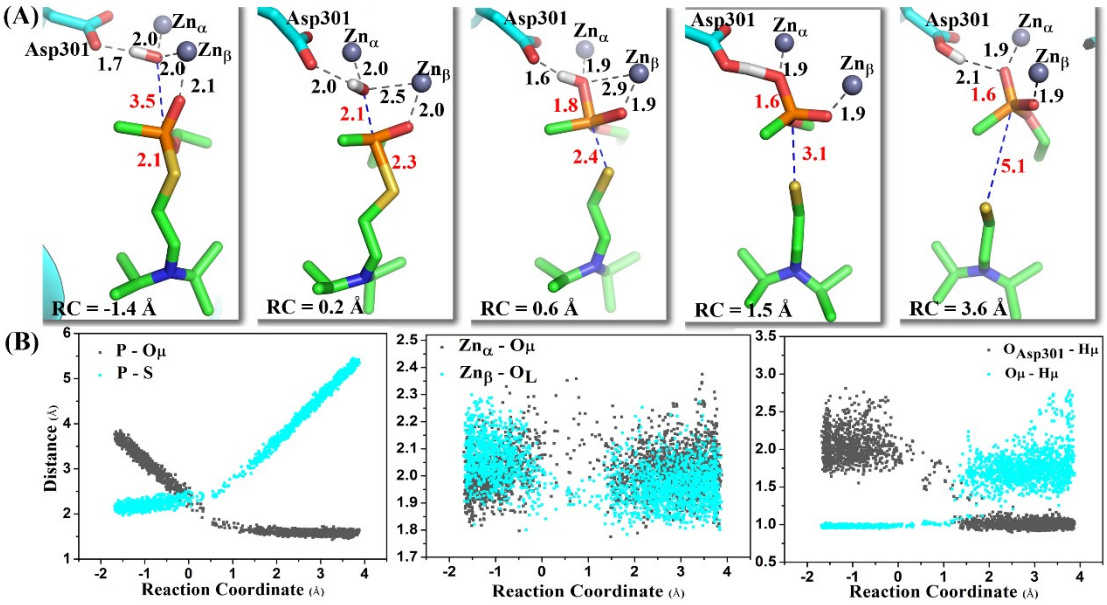

Figure S3 (A) The selected representative structures of the active site in the hydrolytic reaction for S_p-VX-Model A. **(B)** Evolution of selected interatomic distances along the hydrolysis reaction of S_p-VX-Model A.

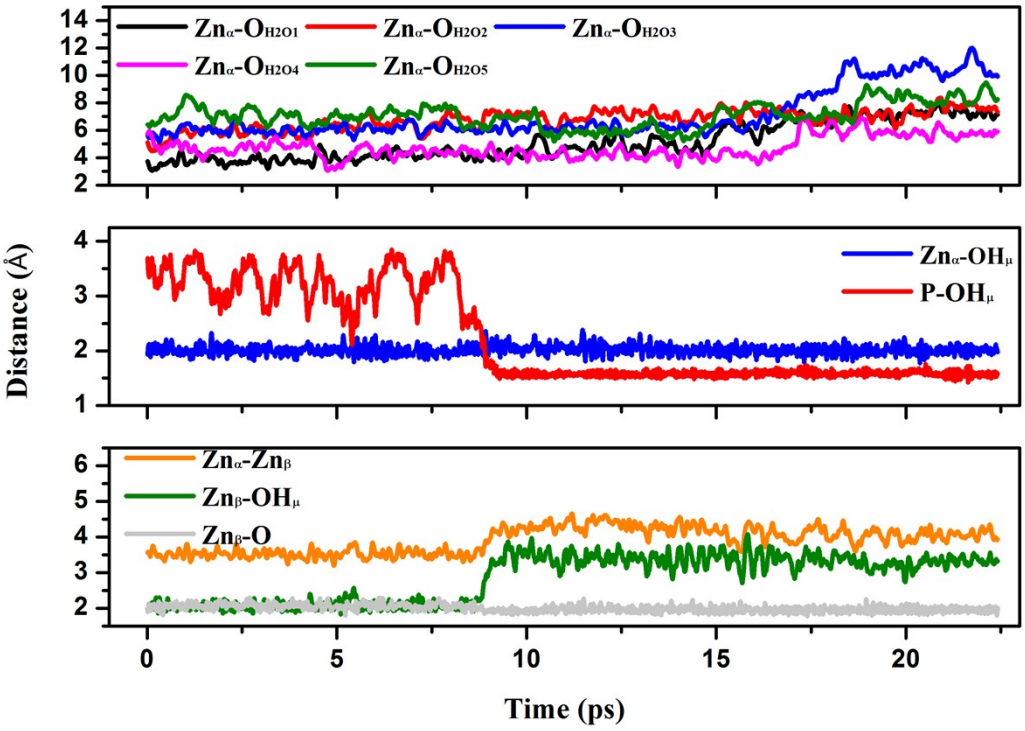

Figure S4 Evolution of selected interatomic distances along the hydrolysis reaction of Sp-VX-model A.

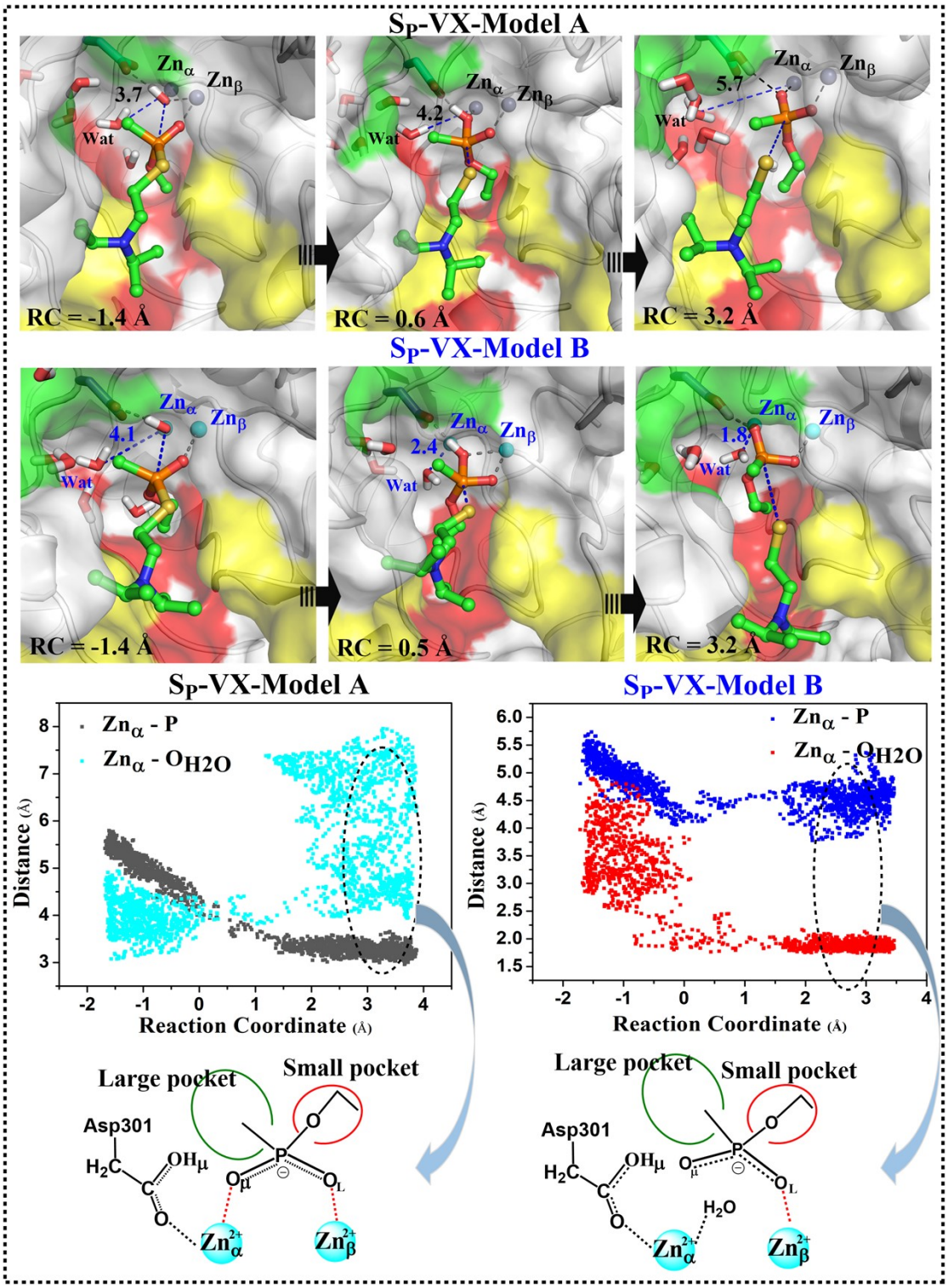

Figure S5. Comparison of the active-site structures and interactions during the hydrolytic process for Models A and B of the S_p-enantiomer.

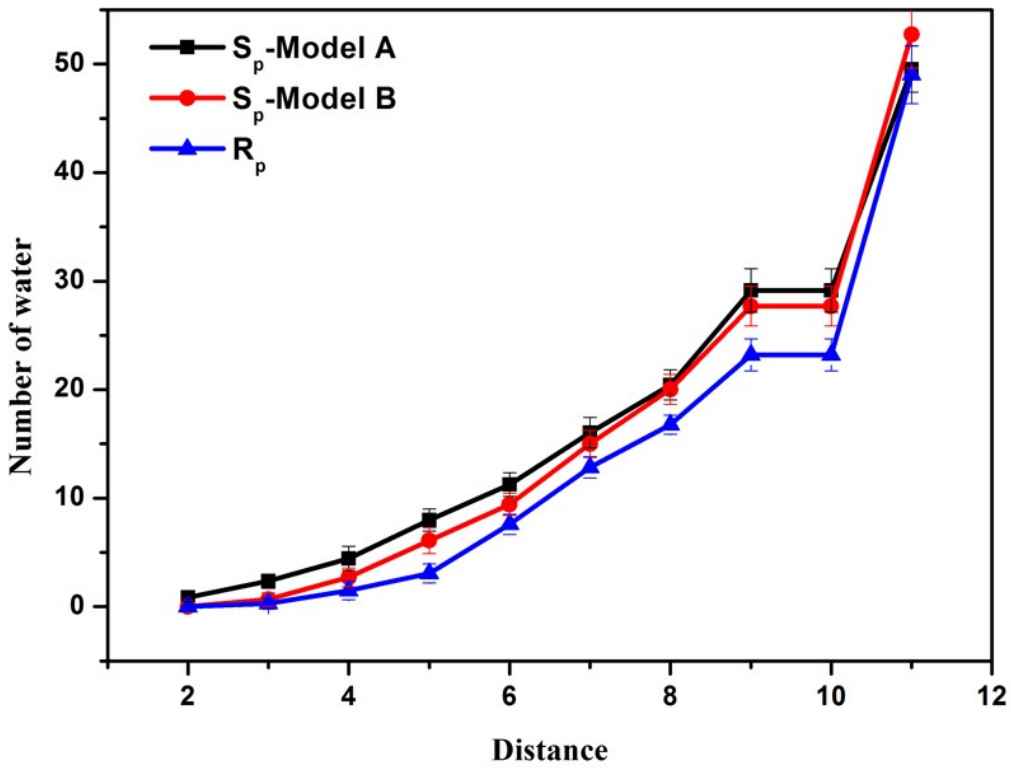

Figure S6 Statistics analysis of water molecules around the binuclear zinc ions within 5 Å for Rp-VX, Sp-VX-Model A and Sp-VX-Model B, respectively.

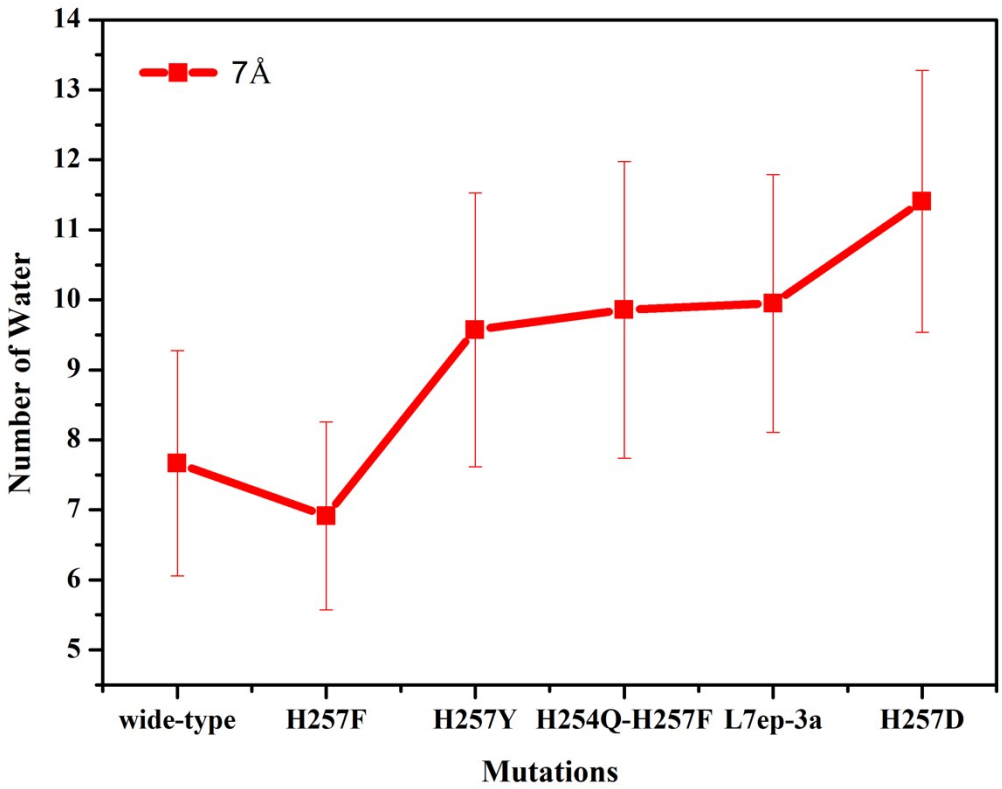

Figure S7 Statistics analysis of water molecules around the binuclear zinc ions within 7 Å for the wide-type and mutants.

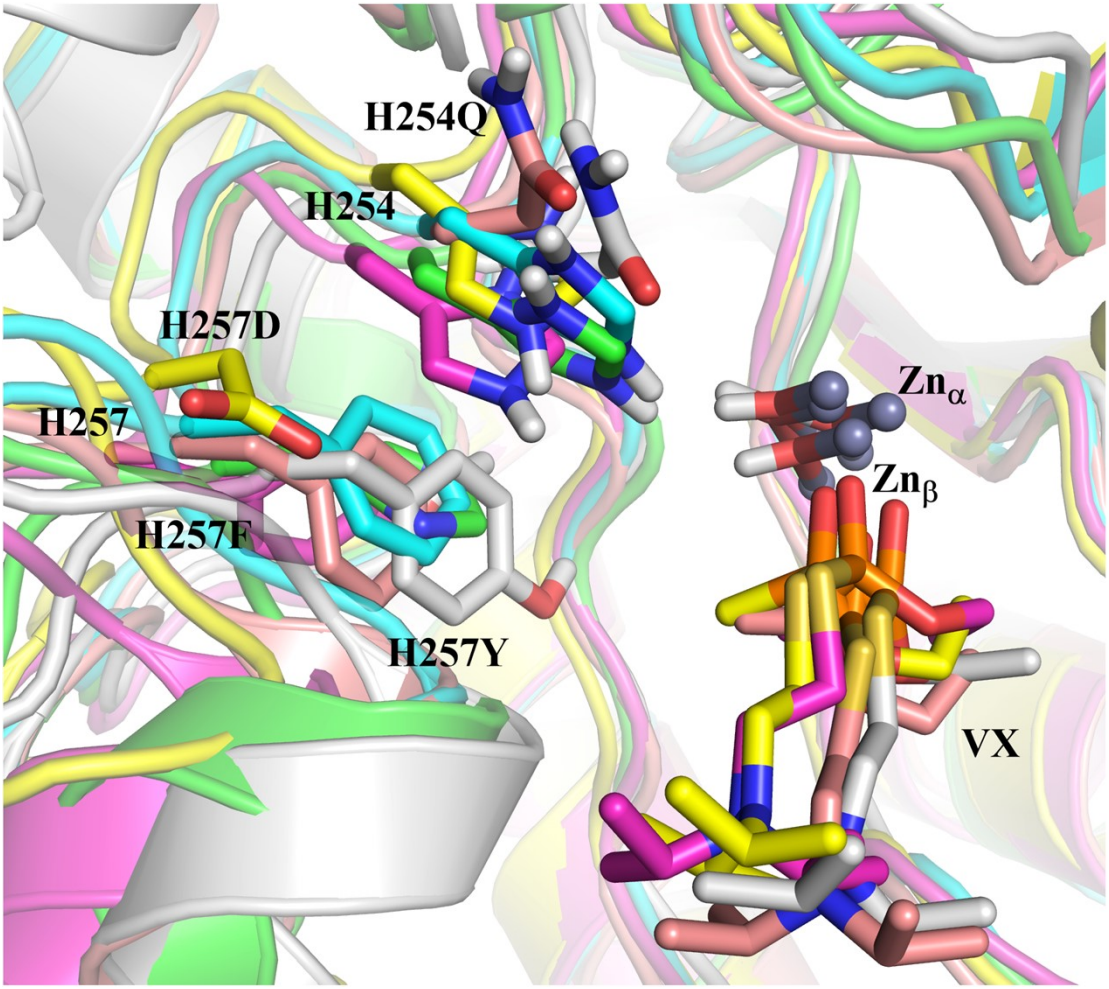

Figure S8. Superimposition of the structure of wide-type (green) and the variant H257F (blue), H257Y (rose red), H254Q-H257F (pink), L7ep-3a (gray), H257D (yellow), where the Zn^{2+} ion is denoted as a purple ball.

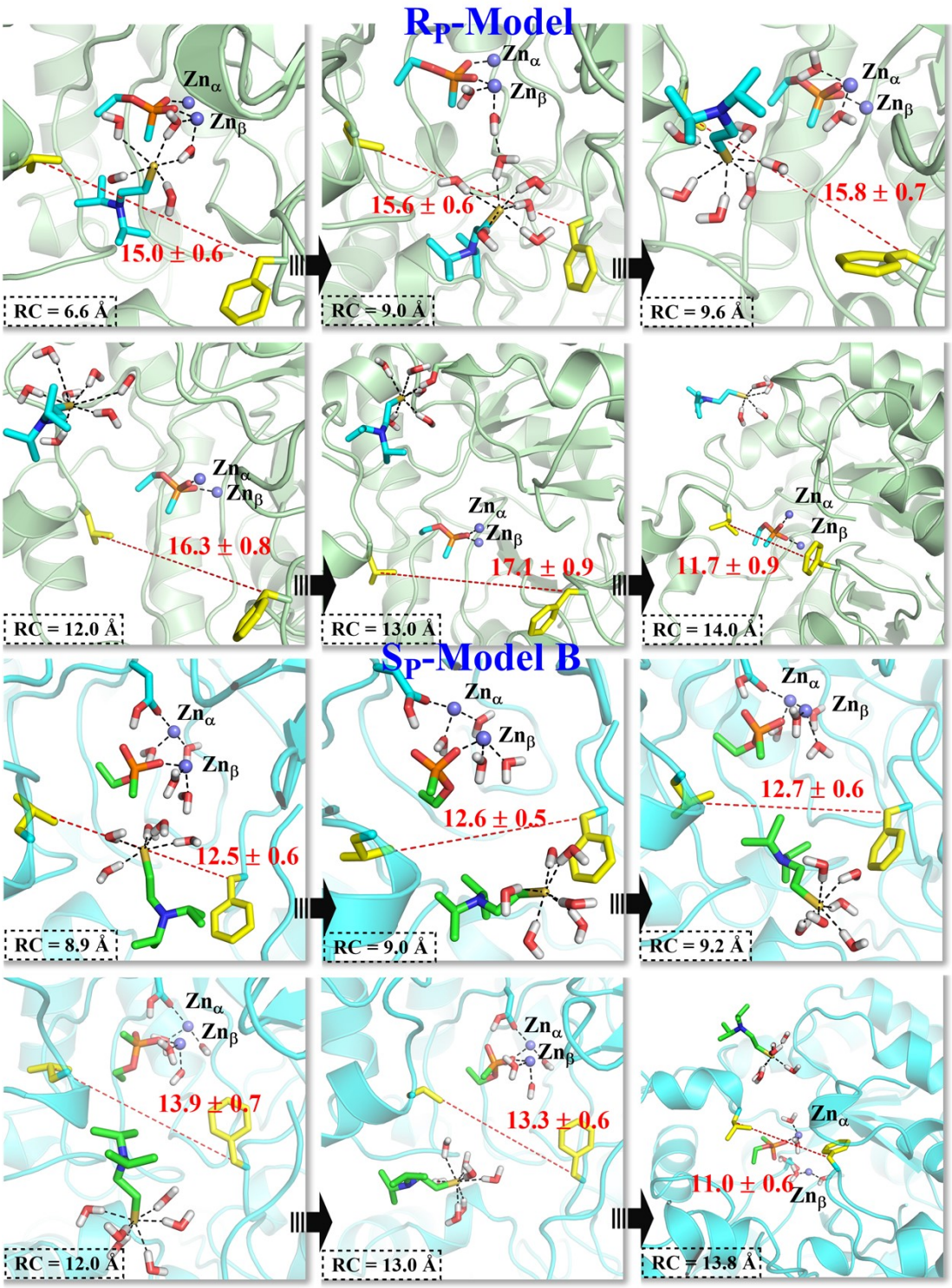

Figure S9 Representative structures and conformational changes of the transportation channel during the release of leaving groups for the substrates Rp-VX and Sp-VX-Model B respectively.

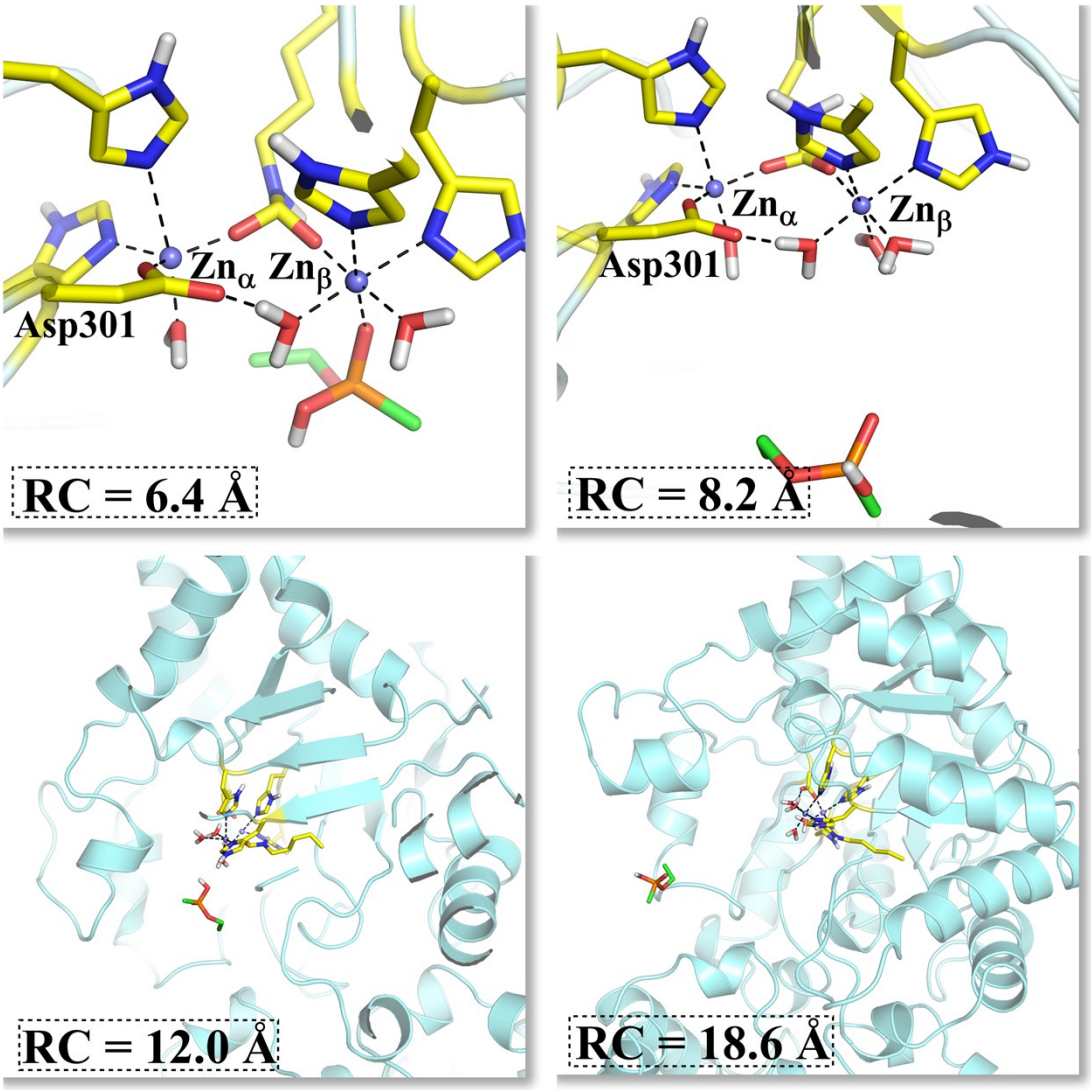

Figure S10 Representative structure and conformational changes of the active domain in PTE for S_P-VX Model B.